STUDY OF AN ELECTRICALLY ANISOTROPIC CYLINDER EXCITED MAGNETICALLY BY A STRAIGHT STRIP LINE

C. A. Valagiannopoulos

School of Electrical and Computer Engineering
National Technical University of Athens
GR 157–73. Zografou, Athens, Greece

Abstract—An infinite homogeneous circular cylinder with full permittivity tensor is excited by a straight strip flowed by arbitrary axial magnetic current. A nontrivial differential equation is derived for the single axial magnetic component which is assigned a plane wave representation. The boundary conditions lead to an integral equation with nonsingular kernel which is solved by supposing a Dirac comb representation for the unknown function. The resultant Green's function multiplied by the current distribution is integrated numerically over the source to give the total field. Various numerical examples are presented and discussed.

1. INTRODUCTION

Electromagnetic devices constructed by anisotropic materials are extensively used and studied for many years. The directional dependent properties are commonly employed to improve devices' operation and performance. In [1], rotating anisotropic elements are used to modify the energy and the frequency of light beams passing through them. A half-wave plate and a linear polarizer are investigated via a non relativistic approach to estimate their effect on an advancing wave train. In [2], the anisotropy in the reception pattern of an antenna is exploited to implement angle-of-arrival measurements techniques. The beam of the receiver antenna is rotated, and the direction corresponding to the maximum signal strength is taken as the direction of the transmitter. Also Dettwiller [3] provides a study concerning the light intensity coming out of a linear anisotropic device. A general expression is received by using Stokes parameters, while conclusions about light polarizations are drawn. Additionally, [4] shows

that the operation of a flat monopole is enhanced by utilizing an anisotropic surface creating coupled resonators. Finally, [5] analyzes a Cartesian layered structure of anisotropic metamaterials using a T-matrix method.

Common occurrences such as substrates of printed circuits, artificial substances, ionospheric layers and composite fluids exhibit certain properties of anisotropy. In this sense, the study of anisotropic materials is crucial as the assumption for isotropic environment is not always realistic. In [6], a solution of the wave functions inside a homogeneous anisotropic medium is given in terms of finite integrals by Ren *et al.*. Interesting properties of the fields defined as a superposition of waves in all the eigenvector directions are discussed and physically interpreted. In [7], a bounded anisotropic environment is investigated and a derivation of the spherical wave functions of all kinds is achieved in terms of an integral representation. In addition, Graglia and Uslenghi [8] obtain the integro-differential equations governing the electromagnetic waves inside a material with arbitrary anisotropy. The region can be three-dimensional and of arbitrary shape. Moreover, in [9] a decoupling of the electromagnetic field inside a general bianisotropic medium is accomplished. Each of the simpler problems possesses a Green's dyad which is analytically determinable. In [12], a version of the Huygens principle inside an anisotropic environment is obtained by parallelizing the two-dimensional original region with a complex isotropic one. Finally, [10] describes the diffraction by an anisotropic half plane, while Sjoberg [11] provides an analysis for the quasi-linear, bianisotropic Maxwell equations using an entropy condition.

Anisotropic rods of circular cross section constitute a special topic which attracts a great amount of attention. This is owed to the analytic properties of the field solutions inside the anisotropic regions. Zhang *et al.* [13] examine a multilayered gyrotropic bianisotropic circular cylinder posed inside free space. A general formulation is presented for the solution of electromagnetic scattering of incident waves using the eigenfunction expansion method. In [14], nonlinear anisotropic circular cylinders are investigated and solutions of scattering of obliquely incident waves are obtained. The nonlinearity problem is overcome by implementing perturbation methods and results for the fundamental frequency components are received. Also in [15], the three-dimensional Green's function of an infinite circular gyroelectric cylinder is derived. Specific analyses concerning excitation of guided modes along the gyroelectric guide and radiation of dipoles in the proximity of the scatterer are provided. In [16], the solutions of the source-free Maxwell's equations in anisotropic media have been developed in terms

of the cylindrical wave functions for isotropic media. Finally, Monzon [17] elaborates the same problem with help of two coupled integral equations with nonsingular kernels and easily obtained solutions.

The aforementioned anisotropic structures can be excited by a variety of sources. In [18], the excitation source for the anisotropic circular cylinder is an embedded monopole and the theoretical conclusions are verified experimentally. In [19] a point source of two alternative polarizations produces field scattered by an anisotropic plasma cylinder. The work deals with the enhancement of the radiation from antennas surrounded by a plasma sheath with axial symmetry. In [20] a plane wave is normally incident to the axis of the anisotropic cylinder. The analysis can be used for oblique wave incidence as well.

The present work investigates an infinitely long circular cylinder which is magnetically inert and electrically anisotropic. The rod is placed inside vacuum area and it scatters the field developed by a straight vertical strip flowed by arbitrary axial magnetic current. The only nonzero magnetic component is the axial one, while the vector of the electric field is parallel to the polar plane. For this reason, the problem is two-dimensional and the dependence of the field functions from the axial coordinate is suppressed. The adopted approach is based on the pioneering paper of Monzon and Damaskos [21].

Application of Ampere's and Faraday's law leads to the formulation of an extended version of Helmholtz differential equation for the axial magnetic field. A plane wave representation with arbitrary complex phases and amplitudes [22–24] is assigned to the unknown function and the explicit expression of the phase is derived. By using again Ampere's law the azimuthal electric field is determined and imposition of boundary conditions results in a couple of integral equations for the amplitude function. We approximate the amplitude by a finite weighted sum of Dirac delta functions and the Green's function is easily specified because the kernel of the integral equation is nonsingular. The total magnetic field is obtained via numerical integration of the product of the magnetic current with the Green's function over the line of the strip.

To validate the correctness of the proposed method and the executed calculations, we check the boundary conditions for several cases. The error is kept very low and the truncation parameters are chosen properly. We examine the effect of the elements of the permittivity tensor on the radiated power and the maximum propagation direction of the device. Various conclusions are drawn and especially the contour plots of the quantities with respect to a couple of real dielectric constants are meaningful and useful. Moreover, the characteristics of the strip source are varied and their influence on the

radiation of the device is observed. The results are discussed and some of them are verified by intuition. Finally, we change the dimensions and the operating frequency of the antenna and we record its response along several rays.

2. PROBLEM FORMULATION

We regard an infinite cylindrical scatterer with circular cross section of radius a. The center of the circle coincides with the origin of the utilized coordinate system. Either Cartesian (x, y, z) or cylindrical (ρ, ϕ, z) coordinates can be used interchangeably. The material of the cylinder (area 1) is magnetically inert and electrically anisotropic with relative permittivity tensor $\bar{\bar{\epsilon}}_1$. A straight strip parallel to the y axis is located external to the rod centralized on the point $(x = b, \ y = 0)$ of the x axis with $a < b$. The strip has a length of $2b \sin \phi_0$ and is flowed by arbitrary z-polarized magnetic current $M_z(\phi)$ (in V/m) as shown in Fig. 1. This current is nonzero only for the angular extent $-\phi_0 < \phi < \phi_0$ with $0 < \phi_0 < \pi/2$. The whole structure is placed inside
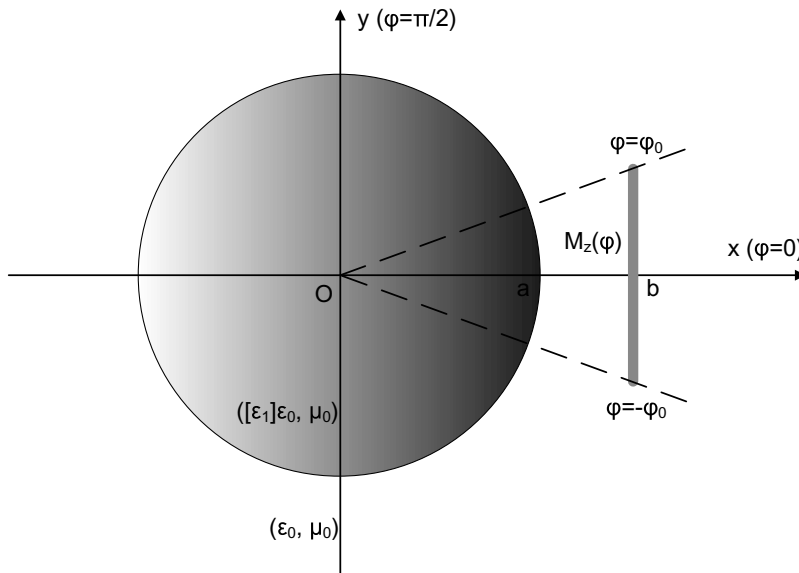

Figure 1. The physical configuration of the device. A straight vertical strip with length $2b \sin \phi_0$ flowed by arbitrary magnetic current $M_z(\phi)$ produces the primary field. It is scattered by a two-dimensional anisotropic cylinder with radius a.

vacuum (area 0). The relative permittivity tensor for the anisotropic material of region 1 is written, in cartesian coordinates, as follows.

$$\overline{\overline{\epsilon}}_1 = \begin{bmatrix} \epsilon_{1xx} & \epsilon_{1xy} & \epsilon_{1xz} \\ \epsilon_{1yx} & \epsilon_{1yy} & \epsilon_{1yz} \\ \epsilon_{1zx} & \epsilon_{1zy} & \epsilon_{1zz} \end{bmatrix} \tag{1}$$

Both the physical configuration and the supposed excitation of the device are invariant across the z axis and consequently the only non vanishing magnetic component is the axial one. In other words, the nature of the problem is two-dimensional and the participating functions are independent of the variable z. Each field quantity is written with a subscript indicating which area it is referred to. The wavenumber and the intrinsic impedance of the vacuum are denoted as (k_0, ζ_0) respectively. A time dependence of the form $e^{+j2\pi ft}$ is adopted and suppressed. The purpose of this work is to compute effectively the far field of the structure. Additionally, the effect of the anisotropy parameters on the radiation pattern of the antenna is interesting to be studied.

3. ANISOTROPIC REGION FIELDS

Let $H_{z1}(x, y)$ stand for the single magnetic component in area 1 and $\{E_{x1}(x, y), E_{y1}(x, y), E_{z1}(x, y)\}$ for the Cartesian electric components inside the cylinder. By application of Ampere's law for the considered anisotropic material, one concludes to the following three scalar equations.

$$\frac{\partial H_{z1}(x, y)}{\partial y} = j\frac{k_0}{\zeta_0} \left[\epsilon_{1xx}E_{x1}(x, y) + \epsilon_{1xy}E_{y1}(x, y) + \epsilon_{1xz}E_{z1}(x, y)\right] \tag{2}$$

$$\frac{\partial H_{z1}(x, y)}{\partial x} = -j\frac{k_0}{\zeta_0} \left[\epsilon_{1yx}E_{x1}(x, y) + \epsilon_{1yy}E_{y1}(x, y) + \epsilon_{1yz}E_{z1}(x, y)\right] \tag{3}$$

$$\epsilon_{1zx}E_{x1}(x, y) + \epsilon_{1zy}E_{y1}(x, y) + \epsilon_{1zz}E_{z1}(x, y) = 0 \tag{4}$$

To this end, we implemented Faraday's law and we found that the partial derivatives of $E_{z1}(x, y)$ with respect to x, y equal to zero. That means that the axial electric component is constant within the anisotropic region. Also from the same law, a relation between the electric components parallel to the polar plane is derived.

$$\frac{\partial E_{y1}(x, y)}{\partial x} - \frac{\partial E_{x1}(x, y)}{\partial y} = -jk_0\zeta_0 H_{z1}(x, y) \tag{5}$$

Solve (4) with respect to $E_{z1}(x, y)$ and substitute it into (2), (3). Use the resulting equations to express $E_{x1}(x, y)$ and $E_{y1}(x, y)$ as functions

of $H_{z1}(x, y)$ derivatives. Finally, eliminate these quantities from (5) to obtain the differential equation below:

$$\left[g_{xx} \frac{\partial^2}{\partial x^2} + (g_{xy} + g_{yx}) \frac{\partial^2}{\partial x \partial y} + g_{yy} \frac{\partial^2}{\partial y^2} + g k_0^2 \right] H_{z1}(x, y) = 0 \qquad (6)$$

The auxiliary quantities appearing above are defined as follows.

$$g_{xx} = \epsilon_{1xz}\epsilon_{1zx} - \epsilon_{1xx}\epsilon_{1zz} \qquad (7)$$
$$g_{xy} = \epsilon_{1xz}\epsilon_{1zy} - \epsilon_{1xy}\epsilon_{1zz} \qquad (8)$$
$$g_{yx} = \epsilon_{1zx}\epsilon_{1yz} - \epsilon_{1yx}\epsilon_{1zz} \qquad (9)$$
$$g_{yy} = \epsilon_{1yz}\epsilon_{1zy} - \epsilon_{1yy}\epsilon_{1zz} \qquad (10)$$

$$g = \epsilon_{1xz}\epsilon_{1yy}\epsilon_{1zx} - \epsilon_{1xy}\epsilon_{1yz}\epsilon_{1zx} - \epsilon_{1xz}\epsilon_{1yx}\epsilon_{1zy}$$
$$+ \epsilon_{1xx}\epsilon_{1yz}\epsilon_{1zy} + \epsilon_{1xy}\epsilon_{1yx}\epsilon_{1zz} - \epsilon_{1xx}\epsilon_{1yy}\epsilon_{1zz} \qquad (11)$$

The differential equation (6) is an extended version of Helmholtz equation which covers anisotropic cases and does not possess an explicit solution. We suppose solutions expressed by means of a plane wave representation. This is an integral of waves with arbitrary complex phases $P(\theta)$ and amplitudes $A(\theta)$ propagating towards all the possible directions θ on x-y plane. This technique is common in bibliography when dealing with nontrivial problems and its advantages are described in [22]. Uzunoglu and Holt [23] adopted this method to specify the field inside an arbitrarily shaped scatterer. Also it is stated [24] that this form is the most general one satisfying the wave equation in a homogeneous material. It should be noted that the phase $P(\theta)$ in the following formula is not related with any direction's wavenumber of area 1, it remains to be determined.

$$H_{z1}(x, y) = \int_{-\pi}^{\pi} A(\theta) e^{-jk_0 P(\theta)(x\cos\theta + y\sin\theta)} d\theta \qquad (12)$$

By replacing (12) in (6), the following expression for $P(\theta)$ is acquired.

$$P(\theta) = \sqrt{\frac{g}{g_{xx}\cos^2\theta + (g_{xy} + g_{yx})\cos\theta\sin\theta + g_{yy}\sin^2\theta}} \qquad (13)$$

Once the phase function is found, it is convenient to rewrite the axial magnetic field in cylindrical coordinates.

$$H_{z1}(\rho, \phi) = \int_{-\pi}^{\pi} A(\theta) e^{-jk_0 \rho P(\theta)\cos(\theta - \phi)} d\theta \qquad (14)$$

The azimuthal electric field $E_{\phi 1}(\rho, \phi)$ inside area 1 should also be specified as it is tangential to the boundary surface of the anisotropic cylinder and therefore is appeared in the relevant boundary condition. The derivation is possible by applying again Ampere's law with use of the transformation formulas [25]:

$$
\begin{bmatrix} E_{1x}(x,y) \\ E_{1y}(x,y) \\ E_{1z}(x,y) \end{bmatrix} = \begin{bmatrix} \cos\phi & -\sin\phi & 0 \\ \sin\phi & \cos\phi & 0 \\ 0 & 0 & 1 \end{bmatrix} \cdot \begin{bmatrix} E_{1\rho}(\rho,\phi) \\ E_{1\phi}(\rho,\phi) \\ E_{1z}(\rho,\phi) \end{bmatrix} \tag{15}
$$

$$
\nabla \times \begin{bmatrix} 0 \\ 0 \\ H_{1z}(\rho,\phi) \end{bmatrix} = \begin{bmatrix} \cos\phi & \sin\phi & 0 \\ -\sin\phi & \cos\phi & 0 \\ 0 & 0 & 1 \end{bmatrix} \cdot \nabla \times \begin{bmatrix} 0 \\ 0 \\ H_{1z}(x,y) \end{bmatrix} \tag{16}
$$

The relation between the unitary vectors of the two coordinate systems is necessary because the tensor of the dielectric constants is given in Cartesian form. The resulting expression is given by

$$
E_{1\phi}(\rho,\phi) = \frac{\zeta_0}{g} \int_{-\pi}^{\pi} A(\theta)P(\theta)e^{-jk_0\rho P(\theta)\cos(\theta-\phi)} \,.
$$
$$
[\cos\theta(g_{xx}\cos\phi + g_{xy}\sin\phi) + \sin\theta(g_{yx}\cos\phi + g_{yy}\sin\phi)]\,d\theta \tag{17}
$$

The amplitude function $A(\theta)$ is still unknown and will be determined by imposing the suitable boundary conditions.

4. SINGULAR MAGNETIC EXCITATION

A prerequisite to proceed analyzing the effect of the strip, is the explicit form of the magnetic-type Green's functions $G_{0/1}(\rho, \phi, R, F)$ inside the corresponding region. A singular magnetic dipole with magnitude $j\zeta_0/k_0$ [26] posed inside area 0 across the axis ($\rho = R, \phi = F$), that is $R > a$, excites the structure. The primary excitation quantity is well-known in series form [27].

$$
G_{0,prim}(\rho,\phi,R,F) = -\frac{j}{4} \sum_{n=-\infty}^{+\infty} e^{jn(\phi-F)} \begin{cases} H_n^{(2)}(k_0R)J_n(k_0\rho), \rho < R \\ J_n(k_0R)H_n^{(2)}(k_0\rho), \rho > R \end{cases} \tag{18}
$$

where $J_n(z), H_n^{(2)}(z)$ are the Bessel and (second type) Hankel functions of order n and argument z. The aforementioned quantity is dimensionless even though it corresponds to the axial magnetic field. It also equals to the electric-type primary Green's function. The

azimuthal electric field is given by

$$G^d_{0,prim}(\rho, \phi, R, F) = \frac{\zeta_0}{4} \sum_{n=-\infty}^{+\infty} e^{jn(\phi-F)} \begin{cases} H_n^{(2)}(k_0 R) J'_n(k_0 \rho), \rho < R \\ J_n(k_0 R) H_n'^{(2)}(k_0 \rho), \rho > R \end{cases}$$

(19)

where the prime $*'$ denotes the differentiation with respect to the entire argument. The secondary responses (magnetic and electric) of the system inside vacuum area 0 possess the following forms.

$$G_{0,sec}(\rho, \phi, R, F) = \sum_{n=-\infty}^{+\infty} C_n(R, F) e^{jn\phi} H_n^{(2)}(k_0 \rho) \tag{20}$$

$$G^d_{0,sec}(\rho, \phi, R, F) = j\zeta_0 \sum_{n=-\infty}^{+\infty} C_n(R, F) e^{jn\phi} H_n'^{(2)}(k_0 \rho) \tag{21}$$

The Hankel functions are the only ρ-dependent components because the region is unbounded and the Sommerfeld's radiation condition should be fulfilled. The respective Green's functions for the anisotropic region 1 are these of (14), (17).

$$G_1(\rho, \phi, R, F) = \int_{-\pi}^{\pi} A(\theta, R, F) e^{-jk_0 \rho P(\theta) \cos(\theta-\phi)} d\theta \tag{22}$$

$$G^d_1(\rho, \phi, R, F) = \zeta_0 \int_{-\pi}^{\pi} A(\theta, R, F) P(\theta) e^{-jk_0 \rho P(\theta) \cos(\theta-\phi)} \Psi(\theta, \phi) d\theta \tag{23}$$

The unknown amplitude $A(\theta, R, F)$ contains inherently the dependency on the source's position (R, F), contrary to the auxiliary quantity $\Psi(\theta, \phi)$ defined below.

$$\Psi(\theta, \phi) = \frac{\cos\theta(g_{xx}\cos\phi + g_{xy}\sin\phi) + \sin\theta(g_{yx}\cos\phi + g_{yy}\sin\phi)}{g} \tag{24}$$

The boundary conditions demand continuity of the tangential field components across the boundary of the scatterer $\rho = a$.

$$G_1(a, \phi, R, F) = G_{0,prim}(a, \phi, R, F) + G_{0,sec}(a, \phi, R, F) \tag{25}$$

$$G^d_1(a, \phi, R, F) = G^d_{0,prim}(a, \phi, R, F) + G^d_{0,sec}(a, \phi, R, F) \tag{26}$$

The z-polarized electric field is also continuous on the cylindrical boundary. This component vanishes into vacuum region and so does in the anisotropic one as $E_{z1}(\rho, \phi)$ does not vary with respect to the observation point. To manipulate the boundary conditions, eliminate the dependence of the azimuthal variable by multiplying (25), (26) by

$e^{-jm\phi}$ for each integer m and integrate with respect to ϕ from $\phi = -\pi$ to π. Via this procedure, we receive the information included in each angular harmonic. If one exploits the orthogonality of the sinusoidal functions, one obtains:

$$\int_{-\pi}^{\pi} A(\theta, R, F) L(\theta, m) d\theta =$$

$$-\frac{j}{4} H_m^{(2)}(k_0 R) J_m(k_0 a) e^{-jmF} + C_m(R, F) H_m^{(2)}(k_0 a) \qquad (27)$$

$$\int_{-\pi}^{\pi} A(\theta, R, F) P(\theta) L_d(\theta, m) d\theta =$$

$$-\frac{j}{4} H_m^{(2)}(k_0 R) J_m'(k_0 a) e^{-jmF} + C_m(R, F) H_m'^{(2)}(k_0 a) \qquad (28)$$

The functions $L(\theta, m), L_d(\theta, m)$ are definite integrals given by

$$L(\theta, m) = \frac{1}{2\pi} \int_{-\pi}^{\pi} e^{-j\gamma(\theta)\cos(\theta-\phi)-jm\phi} d\phi \qquad (29)$$

$$L_d(\theta, m) = -\frac{j}{2\pi} \int_{-\pi}^{\pi} e^{-j\gamma(\theta)\cos(\theta-\phi)-jm\phi} \Psi(\theta, \phi) d\phi \qquad (30)$$

with $\gamma(\theta) = k_0 a P(\theta)$. These integrals are analytically evaluated and expressed in terms of Bessel functions. We simply cite the results, while hints for the derivations are contained in Appendix A.

$$L(\theta, m) = j^{-m} e^{-jm\theta} J_m(\gamma(\theta)) \qquad (31)$$

$$L_d(\theta, m) = \frac{j^{-m} e^{-jm\theta}}{2g}$$
$$\cdot \left[e^{j\theta} \left(\cos\theta(g_{xx} - jg_{xy}) + \sin\theta(g_{yx} - jg_{yy}) \right) J_{m-1}(\gamma(\theta)) \right.$$
$$\left. - e^{-j\theta} \left(\cos\theta(g_{xx} + jg_{xy}) + \sin\theta(g_{yx} + jg_{yy}) \right) J_{m+1}(\gamma(\theta)) \right]$$
$$(32)$$

5. INTEGRAL EQUATION SOLUTION

The integral equation for the unknown function $A(\theta, R, F)$ is formulated by eliminating parameter $C_m(R, F)$ from (28) with help of (27).

$$\int_{-\pi}^{\pi} A(\theta, R, F) \left(P(\theta) L_d(\theta, m) - \frac{H_m'^{(2)}(k_0 a)}{H_m^{(2)}(k_0 a)} L(\theta, m) \right) d\theta =$$
$$\frac{e^{-jmF}}{2\pi k_0 a} \frac{H_m^{(2)}(k_0 R)}{H_m^{(2)}(k_0 a)} \qquad (33)$$

The equation is valid for each integer m. The Wronskian determinant of Bessel functions is used above for simplifying the result. In our consideration we are not so interested in specifying the explicit form of the function $A(\theta, R, F)$, as in determining the field in the anisotropic region. For this reason, we suppose a Dirac comb representation for the unknown function [28] which is possible since the kernel of the integral equation is nonsingular for each $\theta \in (-\pi, \pi)$. With this approach the integrals of (33) for various m are converted to series. The delta functions of the finite sum become infinite at $(2U+1)$ equispaced points $\theta_u = 2u\pi/(2U+1)$ within the integration interval $\theta \in (-\pi, \pi)$.

$$A(\theta, R, F) \cong \sum_{u=-U}^{U} \Delta_u(R, F) \delta(\theta - \theta_u) \qquad (34)$$

Because of the nature of Dirac function we avoided to place delta pulses on the limits of the definition interval. Substitution of (34) in (33) gives the following form:

$$\sum_{u=-U}^{U} \Delta_u(R, F) \left(P(\theta_u) L_d(\theta_u, m) - \frac{H_m^{(2)'}(k_0 a)}{H_m^{(2)}(k_0 a)} L(\theta_u, m) \right) =$$
$$\frac{e^{-jmF}}{2\pi k_0 a} \frac{H_m^{(2)}(k_0 R)}{H_m^{(2)}(k_0 a)} \qquad (35)$$

The unknown weights $\Delta_u(R, F)$ are found by solving the related $(2U+1) \times (2U+1)$ linear system. This is derived by truncating the series (18)–(21) and by restricting the integer indexes n, m to the interval $[-U, U]$. The obtained system is robust and its matrix numerically invertible [21]. Once the coefficients of the sum (34) are determined, substitution to (27) yields to:

$$C_m(R, F) = \frac{1}{H_m^{(2)}(k_0 a)} \cdot$$
$$\left(\frac{j}{4} H_m^{(2)}(k_0 R) J_m(k_0 a) e^{-jmF} + \sum_{u=-U}^{U} \Delta_u(R, F) L(\theta_u, m) \right) \quad (36)$$

for $m = -U, ..., U$. In this way the Green's function for the vacuum area is readily derived:

$$
\begin{aligned}
G_0(\rho, \phi, R, F) &= G_{0,sec}(\rho, \phi, R, F) + G_{0,prim}(\rho, \phi, R, F) \\
&= \sum_{n=-U}^{U} \left(C_n(R, F) - \frac{j}{4} e^{-jnF} J_n(k_0 R) \right) H_n^{(2)}(k_0 \rho) e^{jn\phi}
\end{aligned}
\tag{37}
$$

As far as the primary component of the Green's function is concerned, we choose the formula corresponding to $\rho > R$ for brevity. The expression (37) of $G_0(\rho, \phi, R, F)$ is also suitable for $\rho = R$ because (18) is continuous at the change point.

6. MAGNETIC FIELD INTEGRAL

It is common knowledge that the magnetic field produced by the excited structure is given by the following integral [29]:

$$
H_{z0} = -\frac{jk_0}{\zeta_0} \int_W G_0 M_z dw
\tag{38}
$$

where W is the area of the source (line flowed by magnetic current) and dw the infinitesimal length. The curve of the strip is described in cylindrical coordinates by the polar equation:

$$
\rho = r(F) = b\sqrt{1 + \sin^2 F} \quad , F \in [-\phi_0, \phi_0]
\tag{39}
$$

The explicit form of the equation (38), in the case under consideration, is written as [30]

$$
\begin{aligned}
H_{z0}(\rho, \phi) &= H_{z0,sec}(\rho, \phi) + H_{z0,prim}(\rho, \phi) \\
&= -\frac{jk_0}{\zeta_0} \int_{-\phi_0}^{\phi_0} G_0(\rho, \phi, r(F), F) M_z(F) \sqrt{r^2(F) + r'^2(F)} dF
\end{aligned}
\tag{40}
$$

where a separation between secondary field produced by the cylinder and the primary field in the absence of it, is made. If one replaces the expression of the Green's function of (37) in equation (40), one receives the final form:

$$
H_{z0}(\rho, \phi) = -\frac{jk_0}{\zeta_0} \sum_{n=-U}^{U} H_n^{(2)}(k_0 \rho) e^{jn\phi}
$$

$$
\cdot \int_{-\phi_0}^{\phi_0} \left(C_n(r(F), F) - \frac{j}{4} e^{-jnF} J_n(k_0 r(F)) \right) M_z(F) \sqrt{r^2(F) + r'^2(F)} dF
\tag{41}
$$

The coefficients $C_m(r(F), F)$ in (41) are not analytic with respect to F as the derivation uses a numerical procedure throughout which the position of singularity $(r(F), F)$ is supposed to be invariant. When it comes to the part of integrand of (41), owed to the singular Green's response, a principal function of it is not possible to be found. For these reasons an exact integration is not feasible and a numerical procedure is used instead. The trapezoidal rule is applied for $(2V+1)$ equispaced points within the integration interval $F_v = v\phi_0/V$ for $v = -V, ..., V$. The computation is efficient as the matrix of the linear system (35) determining $C_m(R, F)$ is independent of the location of the source (R, F). Therefore, the trapezoidal integration of (41) requires only one matrix inversion for all the $(2V+1)$ different points of the Green's singularity. The magnetic field in the far region can be determined with use of the following asymptotic relation of Hankel function for large arguments [31, 364]:

$$H_n^{(2)}(k_0\rho) \sim \sqrt{\frac{2}{\pi k_0\rho}} e^{-j(k_0\rho - \frac{n\pi}{2} - \frac{\pi}{4})} \quad , k_0\rho \to +\infty \tag{42}$$

The power radiated by the total, the scattering and the incident electromagnetic waves for observation points in the far region, defined below, will be the main investigated quantities.

$$S(\phi) = \lim_{\rho \to +\infty} \left[\zeta_0 \rho |H_{z0}(\rho, \phi)|^2 \right] \tag{43}$$

$$S_{sec}(\phi) = \lim_{\rho \to +\infty} \left[\zeta_0 \rho |H_{z0,sec}(\rho, \phi)|^2 \right] \tag{44}$$

$$S_{prim}(\phi) = \lim_{\rho \to +\infty} \left[\zeta_0 \rho |H_{z0,prim}(\rho, \phi)|^2 \right] \tag{45}$$

The aforementioned functions have dimensions of power per axial length.

7. NUMERICAL RESULTS

7.1. Parameters and Validation

A set of computer programs has been developed for evaluating the tangential field components on the cylinder's boundary and the far field response of the device. To implement the previously described technique, the truncation parameters should be selected in the first place. As far as the number of the terms U in the delta-function sum (34) is concerned, a careful choice should be made. With increasing U the error of the boundary conditions on the scatterer's surface is

diminished but simultaneously the matrix of the system (35) becomes more and more ill-conditioned. A number of $U = 15$ Dirac function terms per wavelength of the scatterer's perimeter $2\pi a$ leads to robust and physically consistent solutions. When it comes to the number of points V for the application of the numerical (trapezoidal) integrations of (41), the situation is different because with larger V, we always receive more accurate results. A choice that provides convergence for all the near field quantities is using $V = 50$ points per wavelength of strip's length $2b\sin\phi_0$.

The relative permittivity tensor of (1) is not taken to be a full matrix. That is because of the two-dimensional nature of the scattering problem and the fact that the axial electric component E_{z1} is not present. The parameters multiplying this quantity if one expands the definition formula of the electric flux density: $\mathbf{D}_1 = \bar{\bar{\epsilon}}_1 \cdot \mathbf{E}_1$, can be arbitrary but are chosen equal to zero not to affect other operations: $\epsilon_{1xz} = \epsilon_{1yz} = 0$. Moreover, in order to ensure that the axial component of the electric flux density D_{z1} is also vanishing, we take $\epsilon_{1zx} = \epsilon_{1zy} = 0$. The diagonal elements of the tensor (including ϵ_{1zz}) are nonzero, otherwise (4) would be verified even for non vanishing axial electric field E_{z1}. Due to the large number of the problem's parameters, we should assign to some of them typical values which will be kept constant in the following numerical examples if it is not stated differently. For simplicity, we take $\epsilon_{1zz} = 1$ and $a = 3\,\text{cm}$ with $f = 1200\,\text{MHz}$. The strip is usually located at a horizontal distance $b = 5\,\text{cm}$ and its angular extent is chosen equal to $\phi_0 = \pi/7$. The magnetic current flowing the source is generally supposed constant and unitary: $M_z(\phi) = 1\,\text{V/m}$. As far as the observation points in the far region are concerned, the ones corresponding to the direction $\phi = \pi$ are mainly examined. That is because the influence of the rod there is more direct (line-of-sight propagation) and the primary field of the source is not dominant in this region, even for quite small cylinders, due to the device's configuration.

We are permitted to proceed in presenting and observing the effect of the participating parameters on the operation of the investigated device only when the adopted method is validated. In order to test the correctness of the computations and the theoretical completeness of the analyses we represent the errors of the boundary conditions similar to (25), (26) as functions of the azimuthal angle of observation point. Numerical integrations as these of (41) are carried out for the determination of the total error (not only for a single Green's source). A Hermitian permittivity tensor is considered with $\epsilon_{1xy} = -\epsilon_{1yx} = -1.1$, $\epsilon_{1xx} = 3$ and $\epsilon_{1yy} = 2$. The strip is posed at $b = 12$ cm and five different sizes for dielectric rod are examined with $a = 2, 4, 6, 8, 10\,\text{cm}$.

In Figs. 2a and 2b the error is computed in db and it is extremely low (less than -100 db) for both the tangential boundary quantities, a fact that verifies our approach. It is apparent that for cylinders with reduced radii, the error is decreasing because the same number of Dirac functions U is used, while the length of each azimuthal arc in (34) is reduced. In this way, a better representation of the field is achieved. It should be also noted that the error for the electric boundary condition is, in average, larger than this of the magnetic one, as the nature of the problem is magnetic. Moreover, one could notice that the electric boundary condition error exhibits more significant variations with respect to ϕ (maximum at $\phi \cong \pm\pi/3$ and minimum at $\phi \cong 0, \pi$) for smaller rods, whist the opposite happens for the magnetic boundary condition.

7.2. Variable Material Properties

In Fig. 3a we present the far field radiated power $S(\phi)$ along the typical radiation direction $\phi = \pi$ as function of the off-diagonal element of the permittivity tensor ϵ_{1xy} for various ϵ_{1xx}. We suppose $\epsilon_{1yy} = 2.5$ and $\epsilon_{1xy} = \epsilon_{1yx}$ (symmetric matrix). The investigated quantity is dependent only on the magnitude of ϵ_{1xy}, not its sign. Therefore, a symmetry of the curves with respect to the value $\epsilon_{1xy} = 0$ (for which the power is maximized) is observed. Also for decreasing ϵ_{1xx} the decaying behavior away from $\epsilon_{1xy} = 0$ is steeper and the oscillation of the far field greater. Additionally, the minimum value is appeared for larger ϵ_{1xy} as ϵ_{1xx} increases. In Fig. 3b the angle corresponding to maximum propagation power, that is the direction ϕ for which $S_{sec}(\phi)/S_{prim}(\phi)$ becomes maximum, is shown as function of ϵ_{1xy}. One can notice that for a substantial range of ϵ_{1xy} the radiated field is maximized for angles close to $\phi = \pm\pi$ and consequently this direction is worth to be examined (as we did before). The presented functions are odd with respect to the off-diagonal element, while for specific limiting values such as $\epsilon_{1xy} = 0$, discontinuity jumps are detected. These sharp variations happen at the same ϵ_{1xy} for which minimum or maximum far field is appeared in Fig. 3a.

In Fig. 4a the same quantity as in Fig. 3a is represented but for various ϵ_{1yy} with constant $\epsilon_{1xx} = 2.5$. We note that ϵ_{1yy} has a greater impact on the observed field than ϵ_{1xx}. The differences of the curves for different ϵ_{1yy} are larger than the corresponding ones of Fig. 3a, a fact that is explained by the orientation of device's source (parallel to y axis). The power is significantly diminished with decreasing ϵ_{1yy} expressing how strongly the y electric component is weighted inside the anisotropic area. Moreover, for $\epsilon_{1xy} \cong \pm2$ the radiated power is almost vanishing in the case of $\epsilon_{1yy} = 0.5$. In Fig. 4b the same quantity as in
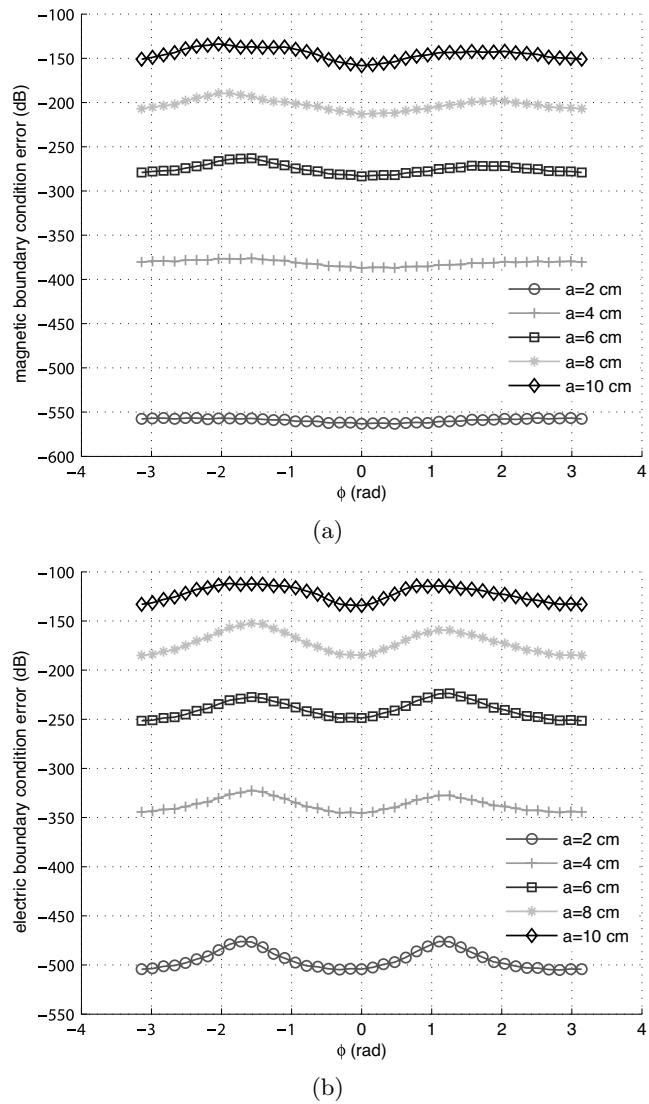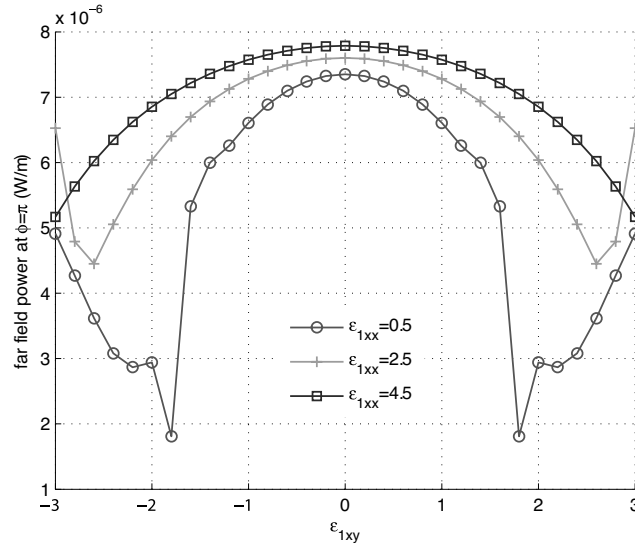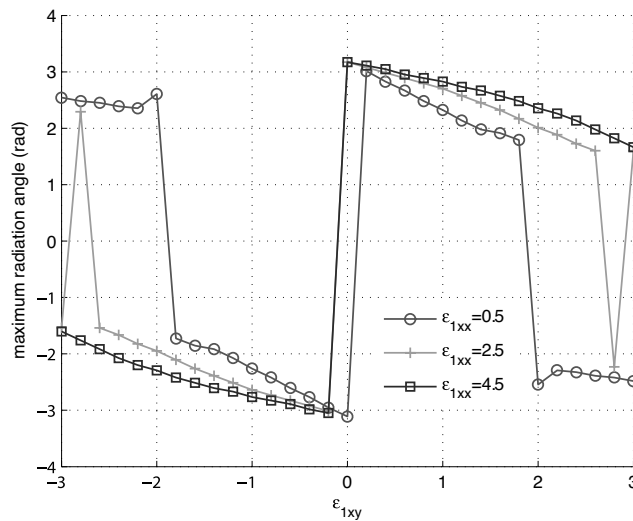
(a)

(b)

Figure 2. The error of the boundary conditions (in db) as function of the azimuthal angle of observation point for various radii of the cylinder: (a) magnetic condition, (b) electric condition. Plot parameters: $\epsilon_{1yx} = -\epsilon_{1xy} = 1.1$, $\epsilon_{1xx} = 3$, $\epsilon_{1yy} = 2$, $\epsilon_{1zz} = 1$, $\epsilon_{1xz} = \epsilon_{1zx} = \epsilon_{1yz} = \epsilon_{1zy} = 0$, $b = 12$ cm, $f = 1200$ MHz, $\phi_0 = \pi/7$, $M_z(\phi) = 1$ V/m.
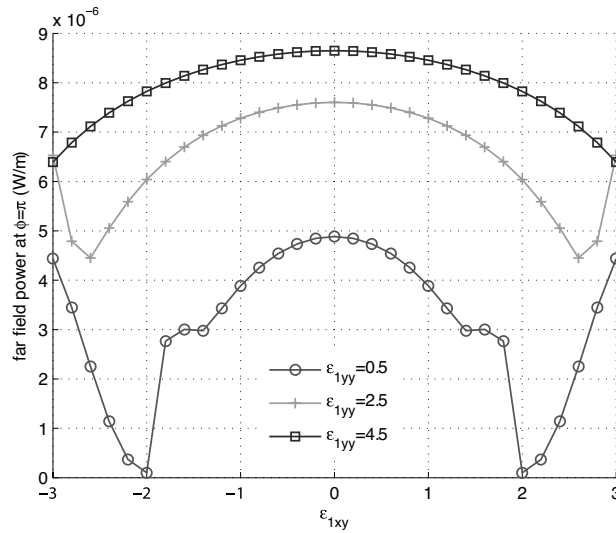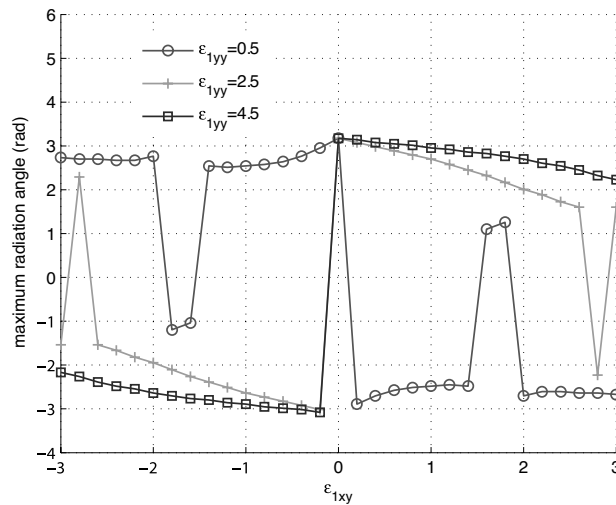
(a)

(b)

Figure 3. The far field radiation as function of the off-diagonal element ϵ_{1xy} of a symmetric tensor for various ϵ_{1xx}: (a) power along the typical ray $\phi = \pi$ in W/m, (b) angle for maximum propagating power in radians. Plot parameters: $\epsilon_{1yy} = 2.5$, $\epsilon_{1zz} = 1$, $\epsilon_{1xz} = \epsilon_{1zx} = \epsilon_{1yz} = \epsilon_{1zy} = 0$, $b = 5$ cm, $f = 1200$ MHz, $\phi_0 = \pi/7$, $a = 3$ cm, $M_z(\phi) = 1$ V/m.
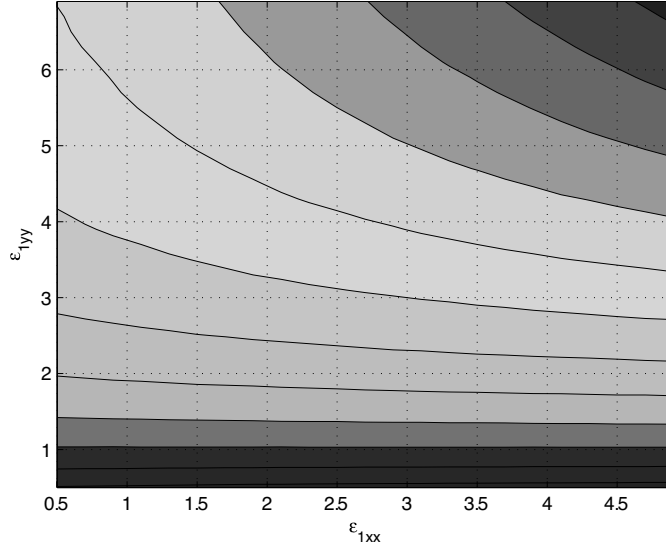
(a)

(b)

Figure 4. The far field radiation as function of the off-diagonal element ϵ_{1xy} of a symmetric tensor for various ϵ_{1yy}: (a) power along the typical ray $\phi = \pi$ in W/m, (b) angle for maximum propagating power in radians. Plot parameters: $\epsilon_{1xx} = 2.5$, $\epsilon_{1zz} = 1$, $\epsilon_{1xz} = \epsilon_{1zx} = \epsilon_{1yz} = \epsilon_{1zy} = 0$, $b = 5\,\text{cm}$, $f = 1200\,\text{MHz}$, $\phi_0 = \pi/7$, $a = 3\,\text{cm}$, $M_z(\phi) = 1\,\text{V/m}$.

Figure 5. The far field radiated power along the typical direction $\phi = \pi$ as function of the diagonal elements ϵ_{1xx}, ϵ_{1yy} of the relative dielectric constants tensor. The material is biaxial. Plot parameters: $\epsilon_{1yx} = -\epsilon_{1xy} = 0$, $\epsilon_{1zz} = 1$, $\epsilon_{1xz} = \epsilon_{1zx} = \epsilon_{1yz} = \epsilon_{1zy} = 0$, $b = 5$ cm, $f = 1200$ MHz, $\phi_0 = \pi/7$, $a = 3$ cm, $M_z(\phi) = 1$ V/m.

Fig. 3b is depicted for several ϵ_{1yy}. In the cases of $\epsilon_{1yy} = 2.5, 4.5$, the variation of the maximum radiation angle is identical to this of Fig. 3b (with a slightly smaller fluctuation). On the contrary, for $\epsilon_{1yy} = 0.5$ the curve is very different not only close to $\epsilon_{1xy} = 0$. In particular, the sign of the angle is inverse, while the jump is replaced by a peak consisted of two discrete measurements. Given the fact that from both sides of this spike the values of the presented quantity are similar, one can guess that the radiated power along the direction indicated by the peak and the other round of it, are almost equal. In other words, a power balance between the two rays is achieved and therefore the maximum direction is difficult to be discerned.

In Fig. 5 we examine the case of a biaxial material with zero off-diagonal elements of its permittivity tensor ($\epsilon_{1xy} = \epsilon_{1yx} = 0$). A contour plot of the radiated power at $\phi = \pi$, $S(\pi)$ is shown, with respect to the diagonal elements which are supposed to be positive ($\epsilon_{1xx}, \epsilon_{1yy}$). It is noticeable that for increasing ϵ_{1yy} with constant ϵ_{1xx}, the far field power increases. This rise is steeper for larger ϵ_{1xx}. The dependence of the measured quantity on ϵ_{1xx} for constant ϵ_{1yy} is much

weaker, and especially for small ϵ_{1yy} the far field is constant. In the case of larger ϵ_{1yy}, the power is an increasing function of ϵ_{1xx} with average value proportional to ϵ_{1yy}.
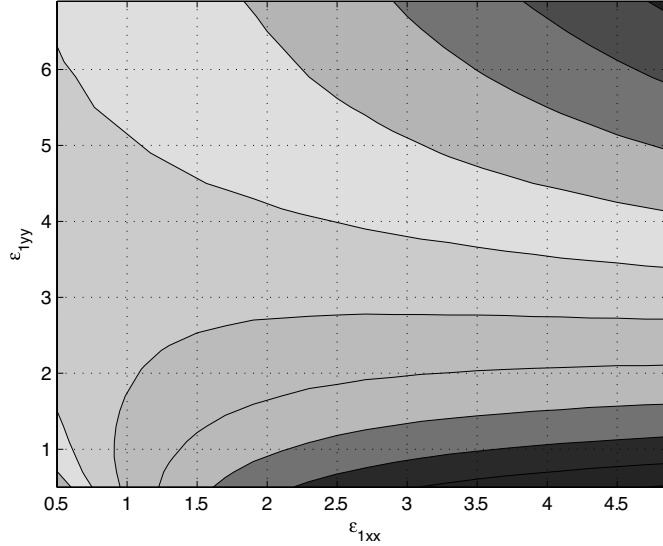

Figure 6. The far field radiated power along the typical direction $\phi = \pi$ as function of the diagonal elements ϵ_{1xx}, ϵ_{1yy} of the relative dielectric constants tensor. The material is gyroelectric. Plot parameters: $\epsilon_{1xy} = -\epsilon_{1yx} = 1.5$, $\epsilon_{1zz} = 1$, $\epsilon_{1xz} = \epsilon_{1zx} = \epsilon_{1yz} = \epsilon_{1zy} = 0$, $b = 5$ cm, $f = 1200$ MHz, $\phi_0 = \pi/7$, $a = 3$ cm, $M_z(\phi) = 1$ V/m.

In Fig. 6 we depict a contour plot of the propagated power along the typical ray $\phi = \pi$, $S(\pi)$ for a gyrotropic material with $\epsilon_{1xy} = -\epsilon_{1yx} = 1.5$, as function of the diagonal elements $(\epsilon_{1xx}, \epsilon_{1yy})$. With constant ϵ_{1yy}, the behavior of the measured quantity is dependent on the parameter ϵ_{1yy} itself. For larger ϵ_{1yy} the far field power increases and for smaller ϵ_{1yy} decreases with respect to ϵ_{1xx}. Within a narrow range near to $\epsilon_{1yy} = 3$, the variation of the quantity is almost negligible. Also for minimum $\epsilon_{1xx}, \epsilon_{1yy}$ a small peak is recorded at the lower left point of the diagram. By keeping constant ϵ_{1xx}, the radiated power is increasing with ϵ_{1yy}. An interesting property is that the fluctuation range of the quantity also increases for greater ϵ_{1xx}, as not only the maximum values are larger but also the minimum ones are smaller.

In Fig. 7 we represent the contour plot of the far field power at $\phi = \pi$, $S(\pi)$ with respect to the off-diagonal elements of the dielectric constant matrix. The material is uniaxial as we suppose $\epsilon_{1xx} = \epsilon_{1yy} =$
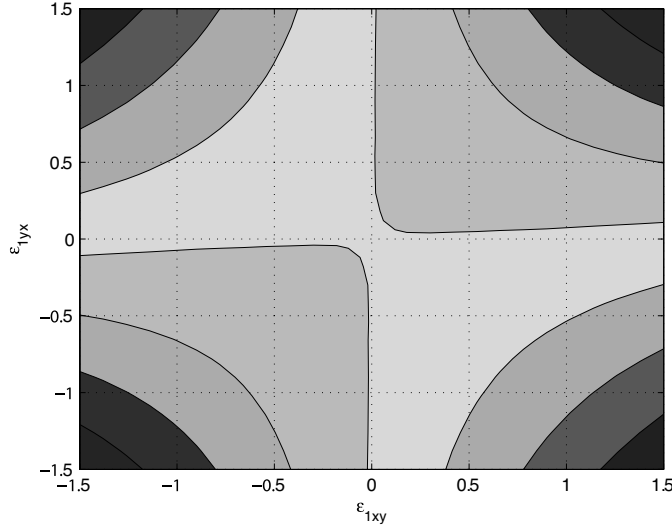
Figure 7. The far field radiated power along the typical direction $\phi = \pi$ as function of the off-diagonal elements ϵ_{1xy}, ϵ_{1yx} of the relative dielectric constants tensor. The material is uniaxial. Plot parameters: $\epsilon_{1xx} = \epsilon_{1yy} = 2.5$, $\epsilon_{1zz} = 1$, $\epsilon_{1xz} = \epsilon_{1zx} = \epsilon_{1yz} = \epsilon_{1zy} = 0$, $b = 5$ cm, $f = 1200$ MHz, $\phi_0 = \pi/7$, $a = 3$ cm, $M_z(\phi) = 1$ V/m.

2.5. One can recognize a saddle point at $(\epsilon_{1xy} = \epsilon_{1yx} = 0)$ when both parameters are vanishing. In the case of a symmetric permittivity tensor $(\epsilon_{1xy} = \epsilon_{1yx})$ a maximum is exhibited, while for gyroelectric material $(\epsilon_{1xy} = -\epsilon_{1yx})$ the same point, coinciding with the origin of the coordinates, constitutes a minimum. It is also noteworthy that the response of the structure is the same when ϵ_{1xy} and ϵ_{1yx} change mutually their positions. Furthermore, for large values of $\epsilon_{1xy}, \epsilon_{1yx}$, the far field at $\phi = \pi$ is vanishing in the symmetric case, while it increases unboundedly in the gyroelectric case.

7.3. Variable Source Position and Current

In Fig. 8a the far field power is appeared as function of the azimuthal angle for various positions b of the excitation source. The radius a is constant and the length of the strip equals $2b \sin \phi_0 = 4$ cm. A symmetric tensor $(\epsilon_{1xy} = \epsilon_{1yx} = 1)$ and a biaxial material $(\epsilon_{1xx} = 2.5, \epsilon_{1yy} = 3)$ are supposed. We observe local maxima at $\phi \cong 0, \pi$, a property that remarks the significance of examining the power channeled towards the typical radiation direction $\phi = \pi$. With
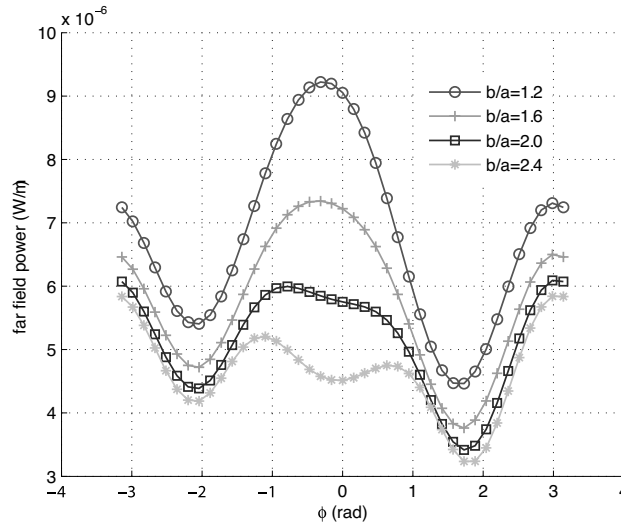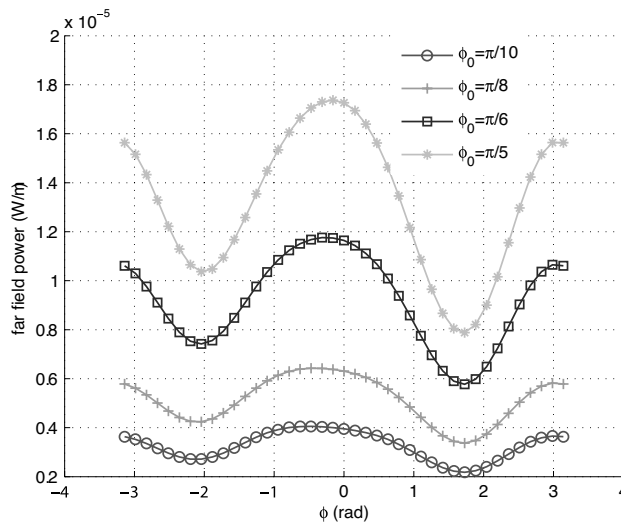
Figure 8. The far field power in W/m as function of the azimuthal angle in radians for various: (a) horizontal positions of the strip $(2b \sin \phi_0 = 4 \, \text{cm})$, (b) angular extents of the strip $(b = 5 \, \text{cm})$. The magnetic current of the source is uniformly distributed. Plot parameters: $\epsilon_{1xx} = 2.5$, $\epsilon_{1yy} = 3$, $\epsilon_{1zz} = 1$, $\epsilon_{1yx} = -\epsilon_{1xy} = 1$ $\epsilon_{1xz} = \epsilon_{1zx} = \epsilon_{1yz} = \epsilon_{1zy} = 0$, $f = 1200 \, \text{MHz}$, $a = 3 \, \text{cm}$, $M_z(\phi) = 1 \, \text{V/m}$.

increasing b the oscillations become more rapid and the response is weaker. The latter is natural because the anisotropic rod close to the strip enforces the radiation operation of the device. Moreover, the dependence of the observed quantity on the position of the source is stronger for observation points close to direction $\phi = 0$. This is explained by the direct influence of the strip to points close to ray $\phi = 0$ as there is no line-of-sight interference by the cylinder. In Fig. 8b the same quantity is presented but for various angular extents $2\phi_0$ of the rod. The curves are not symmetric with respect to $\phi = 0$ due to the directional dependent properties of the scatterer. The greater angular extent is occupied by the strip, the more significant is the response of the device. This is anticipated because for increasing ϕ_0 the length of the strip becomes larger and with constant magnetic current the strength of the source is amplified. Furthermore, the fluctuation of the quantity as function of the azimuthal ϕ angle increases for larger ϕ_0.

The Figs. 9a and 9b correspond to the same configuration of Figs. 8a and 8b with different excitation current defined by the equation $M_z(\phi) = \exp\left[-100\,(\phi/\phi_0)^2\right]$ V/m. The magnetic current is now much more concentrated at $\phi = 0$ (the source similar to a two-dimensional dipole). The magnitudes of the measured power are, in average, 100 times less than in the case of constant unitary current indicated by Figs. 8a and 8b. This is reasonable because now the strength of the source is equivalent to a small fraction of that possessed by the excitation in the previous example. If one ignores the magnitudes, the shape of the curves are almost identical for both the examined cases.

7.4. Variable Device Dimensions

In Figs. 10a, 10b, 10c and 10d we consider a structure with $b = 8$ cm, $\epsilon_{1xx} = 2.5$, $\epsilon_{1xx} = 3$ and $\epsilon_{1xy} = \epsilon_{1yx} = 1.5$. The far field power for four different rays, one normal to the next, $(\phi = -\pi/2, 0, \pi/2, \pi)$ is appeared as function of the radius of the rod for several operating frequencies. In all the regarded cases the quantity exhibits more rapid oscillations with increasing frequency. That is anticipated because the electric size of the device increases. Along the rays $\phi = 0, \pi$, the response of the antenna is more substantial with increasing a and as the operating frequency gets larger the far field gets stronger. Furthermore, for $\phi = -\pi/2$, the values of the curve with $f = 1200$ MHz are greater than these of the $f = 1800$ MHz curve, while the response for the case of $f = 600$ MHz increases rapidly with a. Finally, the radiated power at $\phi = \pi/2$ is maximized for $f = 1800$ MHz and minimized for $f = 1200$ MHz when a possesses a moderate value.
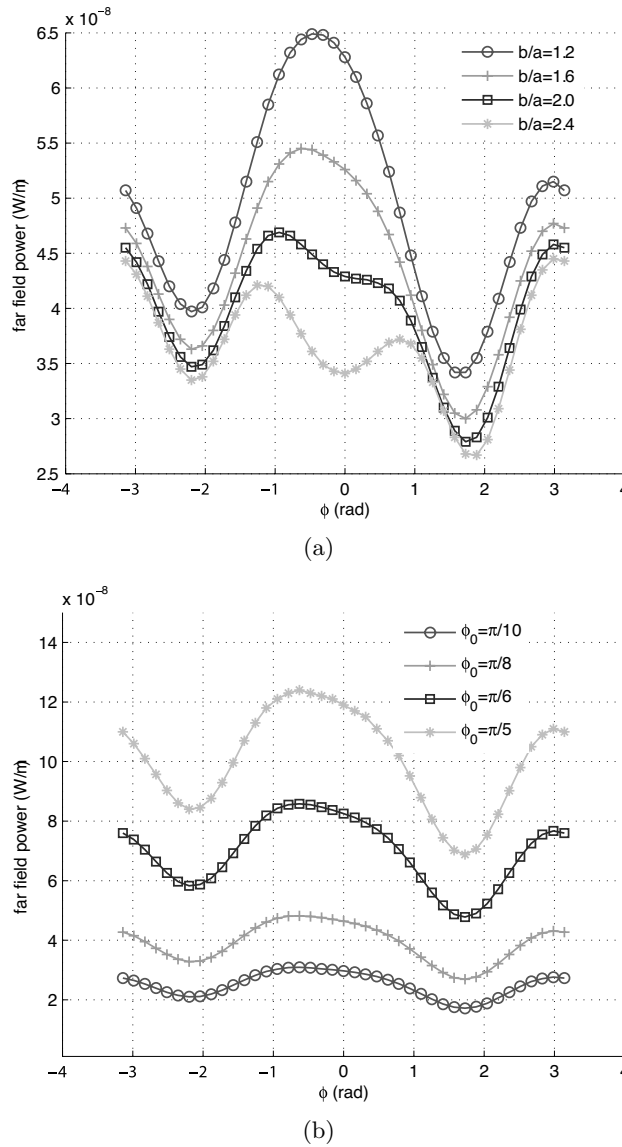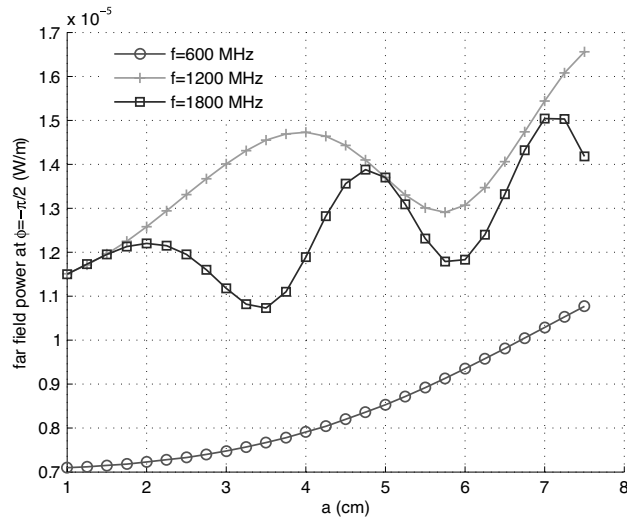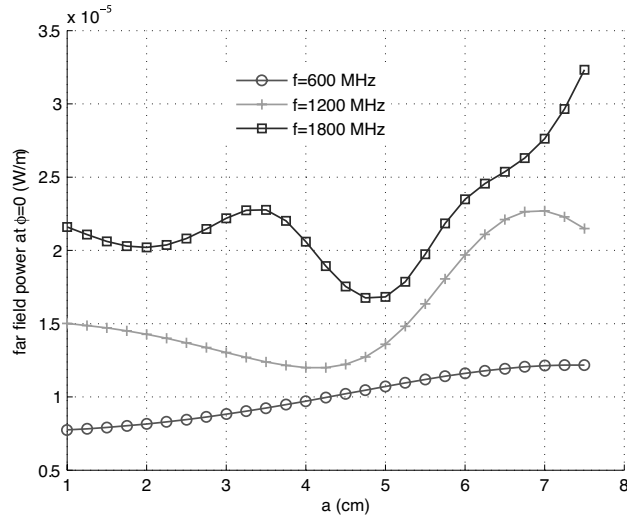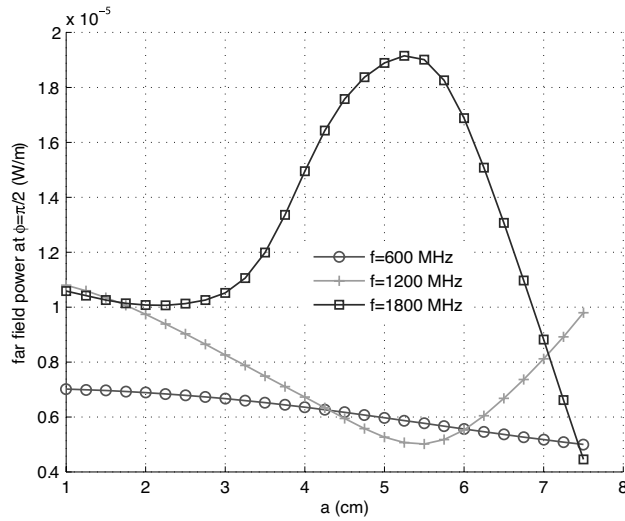
(a)

(b)

Figure 9. The far field power in W/m as function of the azimuthal angle in radians for various: (a) horizontal positions of the strip ($2b \sin \phi_0 = 4$ cm), (b) angular extents of the strip ($b = 5$ cm). The magnetic current of the source is concentrated. Plot parameters: $\epsilon_{1xx} = 2.5$, $\epsilon_{1yy} = 3$, $\epsilon_{1zz} = 1$, $\epsilon_{1yx} = -\epsilon_{1xy} = 1$ $\epsilon_{1xz} = \epsilon_{1zx} = \epsilon_{1yz} = \epsilon_{1zy} = 0$, $f = 1200$ MHz, $a = 3$ cm, $M_z(\phi) = \exp\left[-100 \left(\phi/\phi_0\right)^2\right]$ V/m.
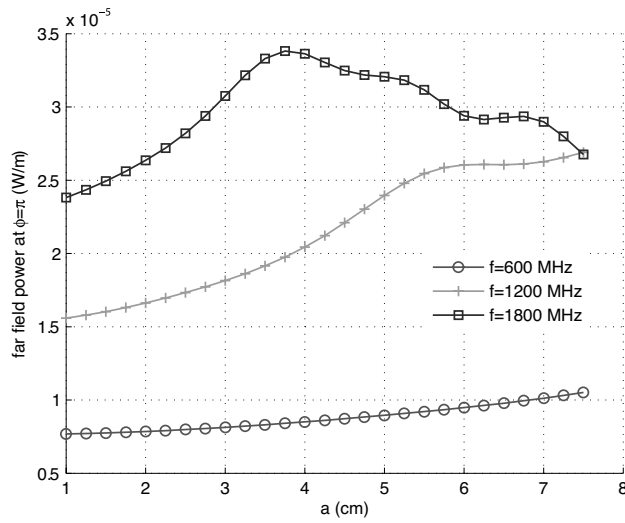
(a)

(b)

(c)

(d)

Figure 10. The far field power in W/m as function of the radius of the cylindrical scatterer for various operating frequencies along the direction: (a) $\phi = -\pi/2$, (b) $\phi = 0$, (c) $\phi = \pi/2$, (d) $\phi = \pi$. Plot parameters: $\epsilon_{1xx} = 2.5$, $\epsilon_{1yy} = 3$, $\epsilon_{1zz} = 1$, $\epsilon_{1yx} = \epsilon_{1xy} = 1.5$, $\epsilon_{1xz} = \epsilon_{1zx} = \epsilon_{1yz} = \epsilon_{1zy} = 0$, $b = 8$ cm, $M_z(\phi) = 1$ V/m.

8. CONCLUSIONS

A homogeneous magnetically inert rod which is electrically anisotropic is the main objective of this study. The structure is proposed to work as antenna and its excitation source is not conformal to the scatterer's surface. A finite strip flowed by arbitrary axial magnetic current (to activate the electrical anisotropy) develops the primary field illuminating the cylinder. The magnetic-type Green's function of the problem is derived by solving an integral equation with nonsingular kernel. The evaluation of the scattering integral over the source is performed numerically and a computationally efficient and convergent solution is obtained. The effect of the position, the length and the current of the strip on the features of the device has been examined. Additionally, the influence of the size of the scatterer and the operating frequency on the operation of the antenna has been observed. But the impact of the permittivity tensor's elements is mainly investigated by using meaningful contour plots.

The proposed technique can be expanded to treat problems with multiple anisotropic cylindrical layers and excitation strips of arbitrary shape. It would be also interesting to investigate the three-dimensional analogous of the problem. Another significant contribution to this work would be the implementation of method of moments for the determination of the current on the strip, while the structure is excited by an elementary source.

APPENDIX A. DERIVATION OF (30) AND (31)

We duplicate a definition of Bessel functions with integer orders n from a standard textbook [31, p. 360, eqn. (9.1.21)]:

$$J_n(z) = \frac{j^{-n}}{\pi} \int_0^\pi e^{jz \cos \theta} \cos(n\theta) d\theta \tag{A1}$$

The integrand function above is even with respect to θ and therefore the integration interval can be converted to symmetric with double length. If one adds to the resulting form the following vanishing quantity

$$-j\frac{j^{-n}}{2\pi} \int_{-\pi}^\pi e^{jz \cos \theta} \sin(n\theta) d\theta = 0 \tag{A2}$$

and take the complex conjugate (for real z), one obtains an alternative definition for Bessel functions of integer orders and real arguments:

$$J_n(z) = \frac{j^n}{2\pi} \int_{-\pi}^\pi e^{-jz \cos \theta + jn\theta} d\theta \tag{A3}$$

By exploiting the azimuthal periodicity of the functions, we make the change of variable $u = \theta - \phi$. It is then straightforward to evaluate (29) and to obtain (31), by taking into account (A3).

As far as the function $L_d(\theta, m)$ of (30) is concerned, convert to exponential form all the harmonic components of $\Psi(\theta, \phi)$ from (24) and make again the change of variable $\phi = \theta - u$. By using the definition (A3) each time we meet a similar integral, four Bessel terms corresponding to orders $m \pm 1$ are obtained. The necessary factoring leads to the two terms of (32).

REFERENCES

1. Bagini, V., F. Gori, M. Santarsiero, F. Frezza, G. Schettini, and G. S. Spagnolo, "Change of energy of photons passing through rotating anisotropic elements," *Eur. J. Phys.*, Vol. 15, 71–78, 1994.

2. Mao, G., B. Fidan, and B. D. O. Anderson, "Wireless sensor network localization techniques," *Computer Networks*, Submitted for publication, 2006.

3. Dettwiller, L., "General expression of light intensity emerging from a linear anisotropic device using Stokes parameters," *Journal of Modern Optics*, Vol. 42, No. 4, 841–848, 1995.

4. Andrasic, G., R. Drewett, I. Morrow, and J. R. James, "New anisotropic monopole bandwidth extension concept," *IEEE Electronics Letters*, Vol. 30, No. 24, 1998–2000, 1994.

5. Grzegorczyk, T. M., X. Chen, J. Pacheco Jr., J. Chen, B.-I. Wu, and J. A. Kong, "Reflection coefficients and Goos-Hanchen shifts in anisotropic and bianisotropic left-handed metamaterials," *Progress In Electromagnetics Research*, PIER 51, 83–113, 2005.

6. Ren, W., X. B. Wu, Z. Yi, and W. G. Lin, "Properties of wave functions in homogeneous anisotropic media," *Physical Review E*, Vol. 51, No. 1, 671–679, 1995.

7. Ren, W., "Contributions to the electromagnetic wave theory of bounded homogeneous anisotropic media," *Physical Review E*, Vol. 47, No. 1, 665–673, 1993.

8. Graglia, R. D. and P. L. E. Uslenghi, "Electromagnetic scattering from anisotropic materials, Part I: General theory," *IEEE Trans. Antennas Propag.*, Vol. 32, No. 8, 867–869, 1984.

9. Lindell, V. and F. Olyslager, "Electromagnetic source decomposition in bianisotropic media," *Journal of Electromagnetic Waves and Applications*, Vol. 12, No. 1, 1–23, 1998.

10. Senior, T. B. A. and E. Topsakal, "Diffraction by an

anisotropic impedance half plane — revised solution," *Progress In Electromagnetics Research*, PIER 53, 1–19, 2005.

11. Sjoberg, D., "On uniqueness and continuity for the quasi-linear, bianisotropic Maxwell equations, using an entropy condition," *Progress In Electromagnetics Research*, PIER 71, 317–339, 2007.

12. Monzon, J. C., "On a surface integral representation for homogeneous anisotropic regions: two-dimensional case," *IEEE Trans. Antennas Propag.*, Vol. 36, No. 10, 1401–1406, 1988.

13. Zhang, M., T. S. Yeo, W. Li, and M. S. Leong, "Electromagnetic scattering by a multilayer gyrotropic bianisotropic circular cylinder," *Progress In Electromagnetics Research*, PIER 40, 91–111, 2003.

14. Hasan, M. A. and P. L. E. Uslenghi, "Electromagnetic scattering from nonlinear anisotropic cylinders—Part I: Fundamental frequency," *IEEE Trans. Antennas Propag.*, Vol. 38, No. 4, 523–533, 1990.

15. Uzunoglu, N. K., P. G. Cottis, and J. G. Fikioris, "Excitation of electromagnetic waves in a gyroelectric cylinder," *IEEE Trans. Antennas Propag.*, Vol. 38, No. 4, 523–533, 1990.

16. Wu, X. B. and K. Yasumoto, "Three-dimensional scattering by an infinite homogeneous anisotropic circular cylinder: an analytical solution," *J. Appl. Phys.*, Vol. 82, No. 5, 1996–2003, 1997.

17. Monzon, J. C., "Three-dimensional scattering by an infinite homogeneous anisotropic circular cylinder: A spectral approach," *IEEE Trans. Antennas Propag.*, Vol. 35, No. 6, 670–682, 1987.

18. Lamensdorf, D. and C.-Y. Ting, "An experimental and theoretical study of the monopole embedded in a cylinder of anisotropic dielectric," *IEEE Trans. Antennas Propag.*, Vol. 16, No. 3, 342–349, 1968.

19. Bichutskaya, T. I. and G. I. Makarov, "Radiation of the point source from an anisotropic plasma cylinder," *Radiophysics and Quantum Electronics*, Vol. 44, No. 8, 616–625, 2001.

20. Ren, W. and X. B. Wu, "Application of an eigenfunction representation to the scattering of a plane wave by an anisotropically coated circular cylinder," *J. Phys. D: Appl. Phys.*, Vol. 28, 1031–1039, 1995.

21. Monzon, J. C. and N. J. Damaskos, "Two-dimensional scattering by a homogeneous anisotropic rod," *IEEE Trans. Antennas Propag.*, Vol. 34, No. 10, 1243–1249, 1986.

22. Clemmow, P. C., *The Plane Wave Spectrum Representation of Electromagnetic Fields*, 3–10, Wiley-IEEE Press, New York, 1996.

23. Uzunoglu, N. K. and A. R. Holt, "The scattering of electromagnetic radiation from dielectric scatterers," *J. Phys. A: Math Gen.*, Vol. 10, No. 3, 413–424, 1977.

24. Stratton, J. A., *Electromagnetic Theory*, 364–365, McGraw-Hill, New York, 1941.

25. Steocker, H. and J. Harris, *Handbook of Mathematics and Computational Science*, 350–353, Springer, New York, 1998.

26. Valagiannopoulos, C. A., "Arbitrary currents on circular cylinder with inhomogeneous cladding and RCS optimization," *Journal of Electromagnetic Waves and Applications*, Vol. 21, No. 5, 665–680, 2007, scheduled for publication.

27. Matthew, N. and O. Sadiku, *Numerical Techniques in Electromagnetics*, 293–294, CRC Press, New York, 2000.

28. Mainguy, S. and J.-J. Greffet, "A numerical evaluation of Rayleigh's theory applied to scattering by randomly rough dielectric surfaces," *Waves in Random Media*, Vol. 8, 89–101, 1998.

29. Nesterenko, M. V. and V. A. Katrich, " The asymptotic solution of an integral equation for magnetic current in a problem of waveguide coupling through narrow slots," *Progress In Electromagnetics Research*, PIER 57, 101–129, 2006.

30. Mauch, S., *Introduction to Methods of Applied Mathematics*, 462–467, 2004, freely available online at http://www.its.caltech.edu/~sean/book.

31. Abramowitz, M. and I. A. Stegun, *Handbook of Mathematical Functions*, National Bureau of Standards, Washington D.C., 1970, freely available online at http://www.math.sfu.ca/~cbm/aands.